See next page for full paper.

THE IMPACT OF CLOUD SHADOWS ON SUBPIXEL TARGET DETECTION

Robert Sundberg

Spectral Sciences, Inc., 4 Fourth Ave., Burlington, MA 01803

ABSTRACT

This paper will examine the impact of cloud shadows on subpixel target detection. When data is collected by a low flying aircraft under partly cloudy skies, there are two main cloud-induced effects: shadowing, which results in diminished and spectrally altered ground illumination, and illumination enhancement of sunlit areas due to the photons scattered from the clouds into these areas. The work presented here examiknes the effects of cloud-induced illumination on the retrieval of reflectance signatures for target detection applications. The impact of cloud shadows is examined using forward simulations of fully and partly shadowed scenes using two hyperspectral reflectance images. One scene contains man-made elements as well as significant areas of vegetation, while the other scene is primarily dry rocky terrain with a region of dark vegetation. Spectral signatures of a blue roof and brown paint were randomly embedded into the two scenes at subpixel levels. The scene radiance is then simulated for fully shadowed, partly shadowed, and fully sunlit conditions. Target detection is performed on these radiance scenes after atmospheric correction. Detection results show improved performance when the sunlit and shadowed areas are segregated and processed independently rather than treating the whole scene at once.

Index Terms— Spectral, simulation, shadow, clouds, visible, infrared

1. INTRODUCTION

The effect of cloud shadows on aerial imagery poses a problem in developing useful data products for agriculture and target detection applications. Shadows affect the ability to compare imagery, including multispectral and hyperspectral imagery (MSI and HSI), taken over periods of time, and the ability to quantify image data analytics. The illumination in cloud shadowed regions includes indirect illumination from a combination of light from the sun filtering through the clouds, and skyshine, the blue-dominated light from the hemisphere of clear sky, which introduces a spectral variation into the shadow. Another effect of clouds is an adjacency effect, which is an additional brightening of directly sunlit areas due to light scattered by cloud edges. Application of retrieval techniques to sunlit areas in the vicinity of broken clouds, even as far as several kilometers away, leads to significant over-prediction of surface reflectance and aerosol optical depth. Several recent papers have examined the impact of 3D clouds on reflectance and aerosol optical depth retrieval [1-5]. This paper examines the effects of cloud shadows on spectral imagery used for target detection.

In this paper, we investigate cloud induced illumination effects using the MODTRAN [6] and MCScene [7-9] codes to forward-simulate cloud shadowed spectral imagery. The basic forward modeling methodology is briefly discussed in Section 2. Section 3 will focus on the effects of cloud shadows on retrieved reflectance, and the use of these reflectance values in target detection algorithms. Section 4 contains a summary of the work presented.

2. FORWARD MODELING OF CLOUD SHADOWS

2.1. MODTRAN-based Modeling Approach

The simulated MODTRAN scenes included a fully sunlit scene and uniform cloud shadows which half-cover or fully cover the scene. The half-shadowed scenes have an abrupt transition between the shadowed and sunlit regions. This abrupt transition would not be found in real imagery where the cloud shadow would show soft edges from cloud optical depth variation, edge effects and the shadow penumbra.

MODTRAN computes line-of-sight (LOS) atmospheric spectral transmittances and radiances over the ultraviolet through long wavelength infrared spectral regime. The radiation transport (RT) physics within MODTRAN provide accurate and fast methods for modeling stratified, horizontally homogeneous atmospheres. The core of the MODTRAN RT is an atmospheric "narrow band model" algorithm. The atmosphere is modeled via constituent vertical profiles, both molecular and particulate, defined using either built-in models, or by user-specified radiosonde or climatology data. The band model provides resolution as fine as 0.2 cm^{-1} from its 0.1 cm^{-1} band model. MODTRAN solves the radiative transfer equation, including the effects of molecular and particulate absorption/emission and scattering, surface reflections and emission, solar/lunar illumination, and spherical refraction.

MODTRAN can be used to generate the appropriate spectral terms to simulate the spectral radiance image for a given scenario and surface spectral reflectance. The observed

spectral radiance, L^*, for a pixel with surface reflectance, ρ, is given by

$$L^* = a\rho/(1-\rho_e S) + b\rho_e/(1-\rho_e S) + L^*_a \quad (1)$$

Here, ρ_e is a spatially averaged surface reflectance, S is the spherical albedo of the atmosphere, L^*_a is the radiance backscattered by the atmosphere, and a and b are coefficients that depend solely on atmospheric and geometric conditions. The values of a, b, S, and L^*_a are determined from MODTRAN simulations. These parameters can be determined for an observing sensor placed below a MODTRAN defined infinite plane-parallel cloud to simulate cloud shadows on the ground.

2.2. MCScene-based Modeling Approach

MCScene, a Direct Simulation Monte Carlo code for 3D atmospheric radiative transfer, can generate complex cloud shadow scenes from 3D cloud models with realistic structure, including thin and thick spots, holes, and the cloud adjacency effect. In the work presented here, a scene was simulated with a cloud shadow covering 2/3 of the image, while direct sunlight illuminated about 1/3 of the image. Figure 1 shows an illustration of the geometry used for the shadowed terrain simulation. The directly illuminated part of the scene also includes photons which have been scattered from the cloud, as well as transmitted through the cloud near the edge of the slab cloud. The shadowed region includes photons which have been scattered through the cloud, along with photons scattered from the atmosphere in to the shadowed region.

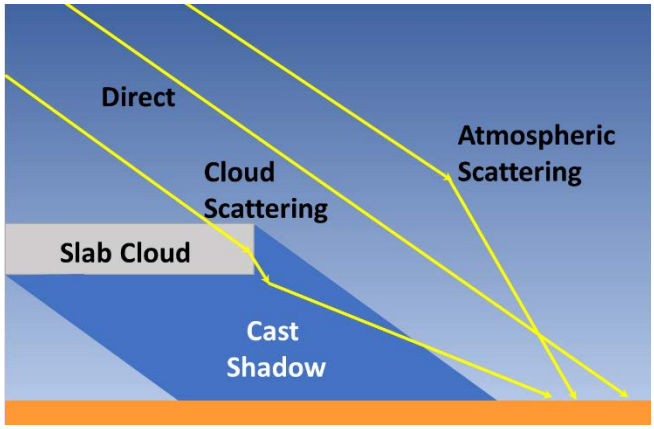

Figure 1. The image illustrates the geometry used in the slab cloud MCScene simulation along with the photon pathways to the directly illuminated region of the terrain.

3. EFFECTS OF CLOUD SHADOWS ON REMOTE SENSING DATA PRODUCTS

3.1. MODTRAN-based Shadow Simulations

Two spectrally different scenes were used in the MODTRAN simulations. They include the Rochester Institute of Technology (RIT) Target Detection Self-Test hyperspectral data, which was part of an airborne HyMap data collect over Cook City, MT [10], and an AVIRIS data collection near Yuma, WA [11]. The Self-Test scene contains a mix of rural and urban areas with several spectrally distinct materials, and the Yuma scene is primarily a dry rocky area with a region of dark vegetation. RGB images of the two atmosphere-free scene reflectances are shown in Figure 2. MODTRAN simulations were performed for shadowed and cloud free conditions for both scenes. The observer was placed at 1 km altitude viewing nadir. Other simulation parameters include a visibility of 23 km and use of MODTRAN's mid-latitude summer atmosphere model. A 1 km thick cumulus cloud was placed over the scene with its base at 2 km altitude, and optical depths of 2 and 30. For these simulations, a full scene average reflectance has been used for ρ_e, the spatially averaged surface reflectance, which simplifies equation (1) to a simple gain and offset applied to every pixel in order to determine the radiance image from the reflectance image.

Figure 2. RGB reflectance images of RIT Target Detection Self-Test scene (top) and the Yuma, WA AVIRIS scene (bottom).

The three simulated radiance scenes, full sunlit, half cloud shadowed, and fully cloud shadowed, have been atmospherically compensated to reflectance units using the QUAC algorithm [12-14]. QUAC is an in-scene approach, requiring only approximate specification of sensor band locations (*i.e.*, central wavelengths) and their radiometric calibration; no additional metadata is required. Because QUAC does not involve first principles RT calculations, it is significantly faster than the physics-based methods and is often used in real-time applications.

3.2. Target Detection Results for MODTRAN-based Simulations

3.2.1 Self-Test Results

For the target detection study, we focused on sub-pixel targets randomly placed throughout the scene. A blue roof spectral signature was extracted from the reflectance image and used as a target signature in the Self-Test scene. The standard Adaptive Coherence/Covariance Estimator (ACE) [15] detector was used to evaluate detection performance for the simulated scenes. Figure 3 shows the receiver-operator curves (ROC) for the detection of 400 subpixel targets varying from a fill-factor of 5% to 45% for a clear-sky case, two half-shadowed cases, and two fully shadowed cases where the cloud shadow was cast by clouds with optical depths of 2 and 30. The fully sunlit and fully shadowed simulations gave very similar detection results, whereas the half-shadowed scenes showed decrease detection performance. There is a clear trend of decreasing performance with increasing cloud optical depth, and therefore decreasing illumination in the shadow region.

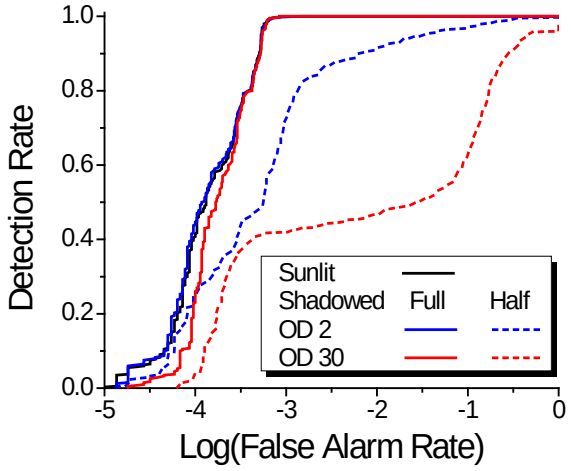

Figure 3. ROC curves for blue roof subpixel targets in the RIT Blind Test Scene using the ACE detection algorithm. The results for the fully sunlit scene (black), fully shadowed scene (labeled full) and half cloud shadowed scenes (labeled half) for cumulus cloud of optical depths of 2 (blue) and 30 (red).

3.2.2 Yuma WA Results

For this scene, a brown paint spectrum was embedded randomly in the scene to represent 400 subpixel targets with fill factors varying from 5% to 25%. The ACE detection results are shown in Figure 4 for fully sunlit, fully shadowed (labeled full) and half-shadowed scenes (labeled half) for cloud optical depths of 2 (blue) and 30 (red). Again, there are improved detection results when the scene is partitioned into sunlit and shadowed regions before being processed, with the half-shadowed scenes showing the lowest detection performance.

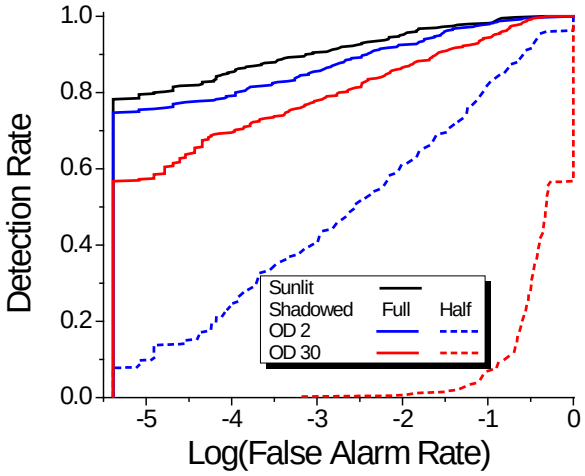

Figure 4. ROC curves for brown paint subpixel targets in the Yuma, WA scene using the ACE detection algorithm. The results for the fully sunlit scene (black), fully shadowed scene (full) and half cloud shadowed scenes (half) for cumulus cloud of optical depths of 2 (blue) and 30 (red).

3.3. MCScene-based Shadow Simulations

For this initial study, a simple slab cloud model, see Figure 1, was used to produce a uniform cloud which cast a shadow over 2/3 of the central part of the RIT Self-Test reflectance scene. Figure 5 shows the RGB radiance images of a cloud free scene (top) and 2/3 shadowed scene (bottom), a linear stretch was used in this image to emphasize the shadowed region of the scene. The MCScene simulations were performed with an observer placed at 20 km altitude viewing nadir. Other simulation parameters include a rural aerosol with a visibility of 23 km and use of MODTRAN's mid-latitude summer atmosphere model. A 1 km thick cumulus cloud was placed to the west of the scene with its base at 2 km altitude, and an optical depth of 10. A solar zenith angle of 20 degrees with the sun due west produced a cloud shadow over roughly 2/3 of the scene. This simulation includes the soft edge of the cloud shadow due to the varying thickness of the optical path through the cloud near the edge of the cloud and a 1-pixel gaussian blur to represent sensor optical blur.

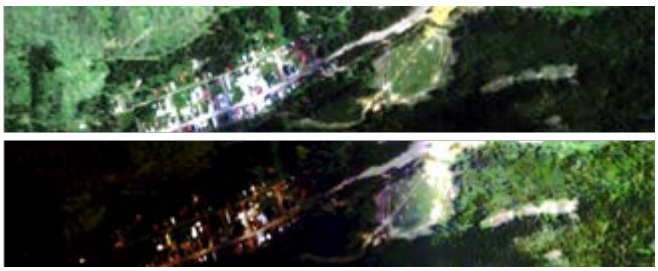

Figure 5. RGB radiance images simulated by MCScene for a subset of the RIT Target Detection Self-Test scene for cloud-free (top) and a 2/3 cloud shadowed scene (bottom).

3.4 Target Detection Results for MCScene-based Simulations

The ROC curves using the ACE detector for the blue roof spectrum detected in the MCScene generated scene is shown in Figure 6. The detection algorithm was run on the whole scene, labeled half shadow, and then run separately on the left and right thirds of the scene to capture the complete shadow and sunlit regions. Segregating the scene into sunlit and shadowed regions before atmospheric correction and detection produces better detection results.

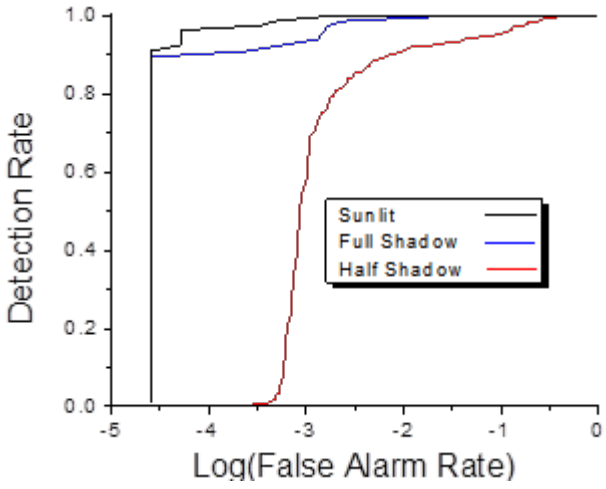

Figure 6. ROC curves for blue roof subpixel targets in the RIT Blind Test Scene simulated by MCScene using QUAC atmospheric correction followed by the ACE detection algorithm. The results for the sunlit part of the scene (black), shadowed part of the scene (blue) and the combined shadowed and sunlit scene (red).

In Figure 7, we compare the ACE detection images for the sunlit part of the scene. The top detection image is the result when the full scene is processed containing both the shadowed and sunlit regions. This detection image shows missed or weakly detected targets, pointed to with red arrows, which were successfully detected when the sunlit part of the scene is processed separately.

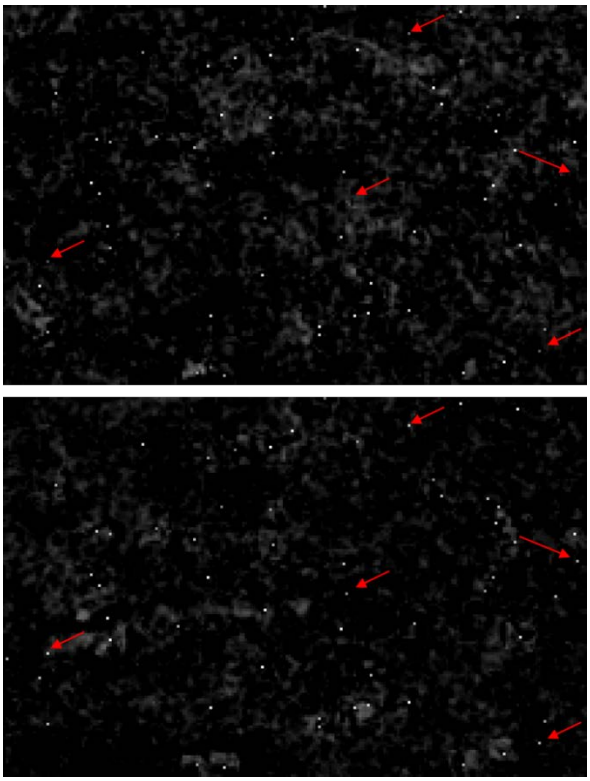

Figure 7. ACE detection images for the sunlit portion of the MCScene simulated image when the whole image is processed (top) and when the sunlit part of the image is processed separately (bottom). The red arrows in both images point to targets which were not strongly detected in the top image.

4. CONCLUSIONS

This study has used MODTRAN and MCScene radiation transport simulations of cloud-free and cloudy conditions to investigate the impact of cloud shadows on target detection. Radiance scenes were simulated for half-shadowed, fully shadowed, and clear-sky conditions using MODTRAN. Blue roof and brown paint spectra were embedded into hyperspectral reflectance scenes as subpixel targets. The simulated radiance scenes were atmospherically corrected to reflectance using QUAC, and then target detection was performed using the ACE detector. The performance of the target detection algorithms was degraded significantly when cloud shadows and sun illuminated regions were processed to reflectance without segregation into separate regions. MCScene simulations showed similar target detection trends. In these simulations a slab cloud was used to produce shadowed and sunlit regions using part of the RIT Self-Test scene with blue roof subpixel targets. Partitioning the scene into sunlit and shadowed regions before processing produced better detection performance. Future simulations will examine the impact of more complex cloud shadows cast by realistic 3D clouds on target detection and agricultural data products.

ACKNOWLEDGMENT

The author wishes to acknowledge Spectral Sciences, Inc. for support under an internal research and development grant.

5. REFERENCES

[1] S. Richtsmeier and R.L. Sundberg, "Full spectrum cloud scene simulation," *IEEE International Geoscience & Remote Sensing Symposium*, Melbourne, Australia, (July 21-26, 2013).

[2] G. Wen, A. Marshak, and R. Cahalan, "Impact of 3D clouds on clear sky reflectance and aerosol retrieval in a biomass burning region of Brazil," *J. Geophys. Res.* 112:.D13204 (2006).

[3] A. Marshak, G. Wen, J. Coakley, L. Remer, N. Loeb, and R. Cahalan, "A simple model for the cloud adjacency effect and the apparent bluing of aerosols near clouds," *J. Geophys. Res.* 113:D14S17 (2008).

[4] E. Kassianov and M. Ovtchinnikov, "On reflectance ratios and aerosol optical depth retrieval in the presence of cumulus clouds," *J. Geophys. Res. Lett.* 35: L06807 (2008).

[5] E. Kassianov, M. Ovtchinnikov, L. Berg, S. McFarlane, and C. Flynn, "Retrieval of aerosol optical depth in vicinity of broken clouds from reflectance ratios: sensitivity study," *JQSRT*, doi:10.1016/j.jqsrt.2009.01.014 (2009).

[6] A. Berk, P. Conforti, R. Kennett, T. Perkins, F. Hawes, and J. van den Bosch, "MODTRAN6: a major upgrade of the MODTRAN radiative transfer code," *Proc. SPIE, Algorithms and Technologies for Multispectral, Hyperspectral, and Ultraspectral Imagery XX*, 90880H (June 13, 2014); doi:10.1117/12.2050433.

[7] S.C Richtsmeier, D.K Lynch, and D.S.P. Dearborn, "Antitwilight II: Monte Carlo simulations," *Applied Optics* 56, G169--G178 (2017); doi: 10.1364/AO.56.00G169.

[8] R.L. Sundberg and S. Richtsmeier, "Reflectance retrieval in the presence of optically opaque broken clouds," in *IEEE GRSS Workshop on Hyperspectral Image and Signal Processing: Evolution in Remote Sensing (WHISPERS)*, 6th Workshop (2014).

[9] S. Richtsmeier, A. Singer-Berk, and R.L. Sundberg, "Full spectrum cloudy scene simulation," *SPIE Proceedings, Algorithms and Technologies for Multispectral, Hyperspectral, and Ultraspectral Imagery XVI*, Vol. 7695, doi: 10.1117/12.850874 (2010).

[10] J.P. Kerekes and D.K. Snyder, "Unresolved target detection blind test project overview," *Proc. of SPIE* Vol. 7695 769521-1 (2010).

[11] R.O. Green, M.L. Eastwood, C.M. Sarture, T.G. Chrien, M. Aronsson, B.J. Chippendale, J.A. Faust, B.E. Pavri, C.J. Chovit, M. Solis, M.R. Olah, and O. Williams, "*Imaging spectroscopy and the Airborne Visible/Infrared Imaging Spectrometer (AVIRIS)," Remote Sensing of Environment*, 65: 227-248 (1998).

[12] L.S. Bernstein, X. Jin, B. Gregor, and S. Adler-Golden, "The Quick Atmospheric Correction (QUAC) code: algorithm description and recent upgrades," *Opt. Eng*. 51(11), 111719 (2012).

[13] L.S. Bernstein, S.M. Adler-Golden, R.L. Sundberg, and A.J. Ratkowski, "In-scene-based atmospheric correction of uncalibrated VISible-SWIR (VIS-SWIR) hyper- and multispectral imagery," *Proc. SPIE Int. Soc. Opt. Eng.*, 7107 (2008).

[14] L.S. Bernstein, S.M. Adler-Golden, R.L. Sundberg, R.Y. Levine, T.C. Perkins, A. Berk, A.J. Ratkowski, G. Felde, and M.L. Hoke, "Validation of the QUick atmospheric correction (QUAC) algorithm for VNIR-SWIR multi- and hyperspectral imagery," *Proc. SPIE Int. Soc. Opt. Eng.*, 5806, pp. 668-678 (2005).

[15] S.S. Kraut, L.L. Scharf, and R.W. Butler, "The Adaptive Coherence Estimator: A uniformly most-powerful invariant adaptive detection statistic," *IEEE Trans. Signal Processing*, Vol. 53, No. 2 (2005).